REINFORCEMENT OF THE 18TH CENTURY BUTTRESSES OF MANIACE CASTLE: DESIGN AND EXECUTION

Figure 1 Overview of Maniace Castle on the tip of Ortygia island.

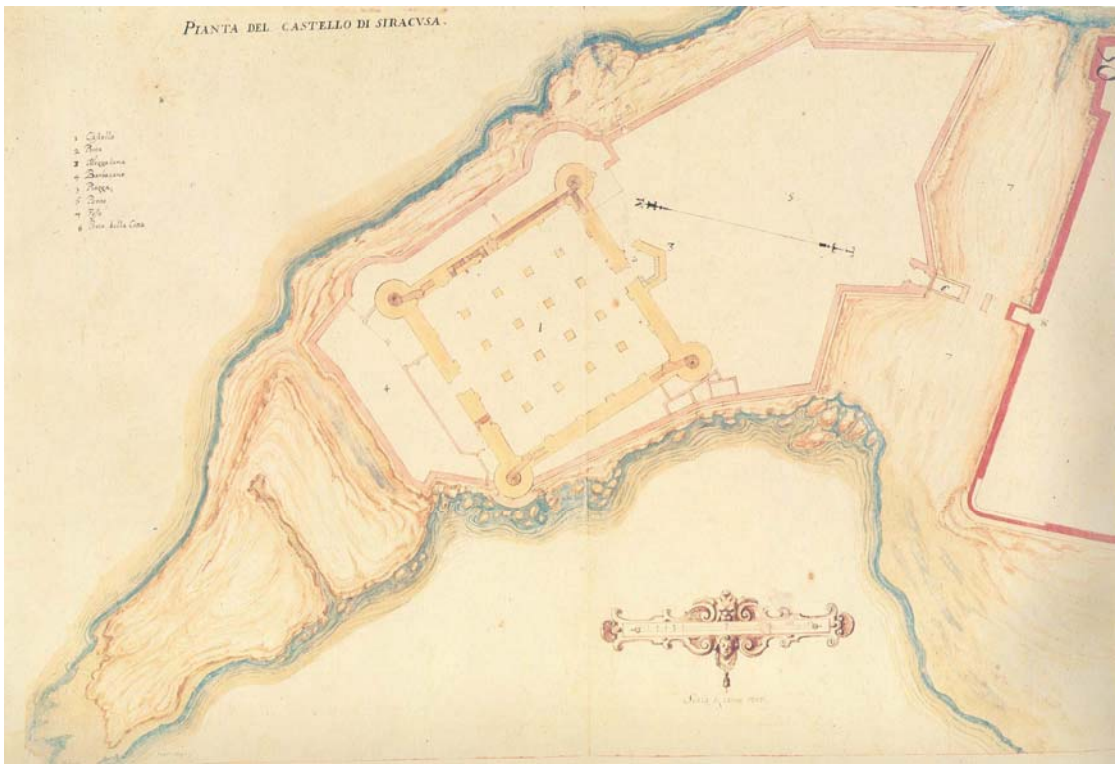

Figure 2 Plan of the great hypostyle hall of the Castle (Salone) in a 1640 drawing by F. Negro (Bares 2011).

Figure 3 Restoration works on the cross vaults of the *Salone* carried out after the 1693 earthquake, involving the replacement of the original web stones by lighter lava stones.

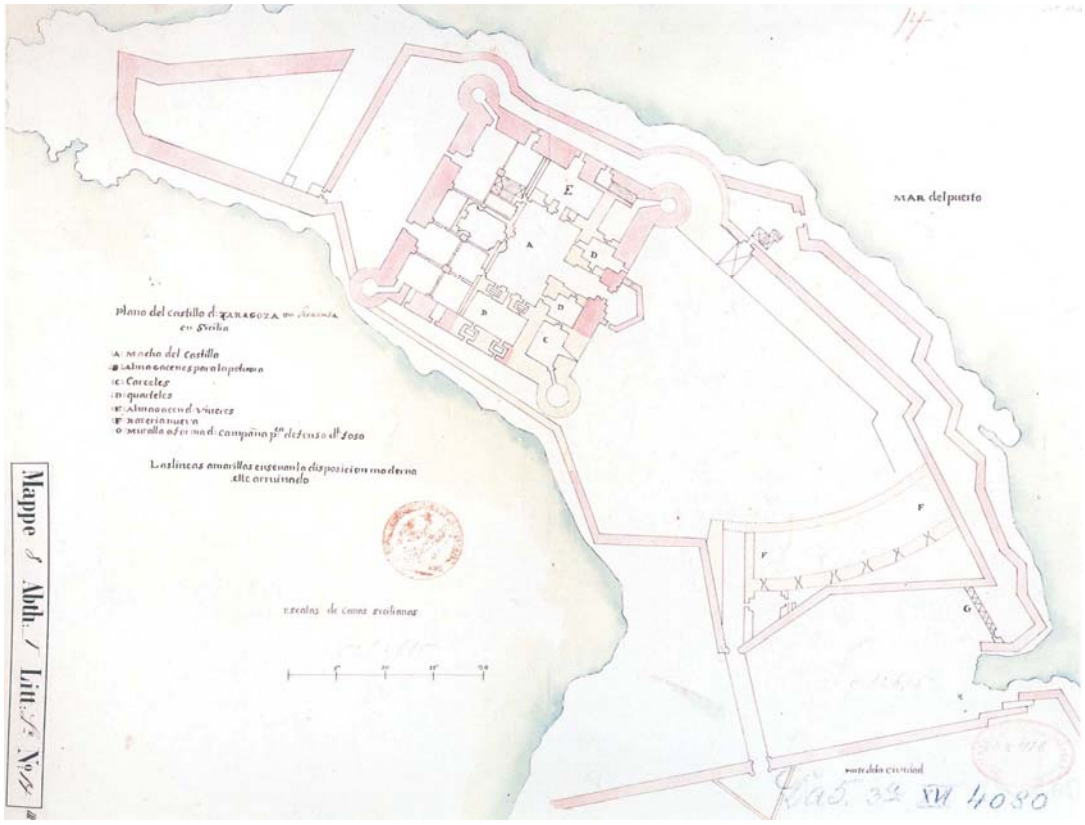

Figure 4 Plan of a project proposal after the explosion of the ammunition dump in 1704 (Bares 2011); the Castle layout seems comparable to one at present, with differences revealing further adjustments introduced in the following century.

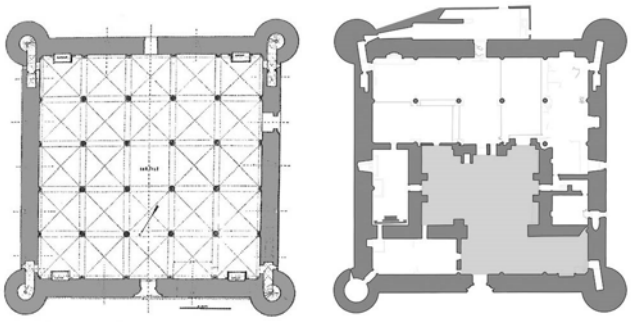

Figure 5 Comparison between the original layout (left) of the *Salone* according to G. Agnello (Bares 2011) and its present configuration (right) in the general survey by the Superintendence of Siracusa.

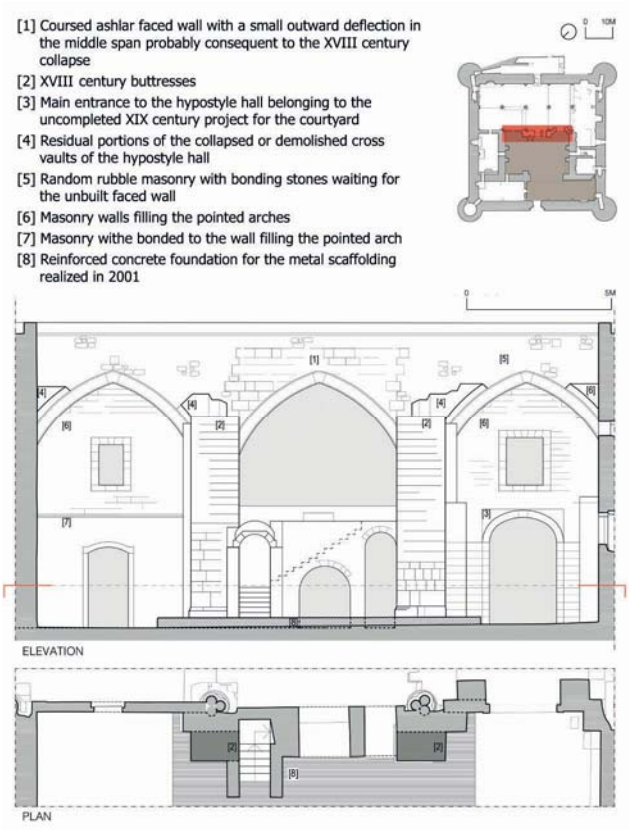

Figure 6 Plan and elevation of the façade overlooking the inner courtyard of the Castle with the two buttresses built in the XVIII century to counteract the thrust of the surviving vaults of the hypostyle hall springing from the trilobate columns.

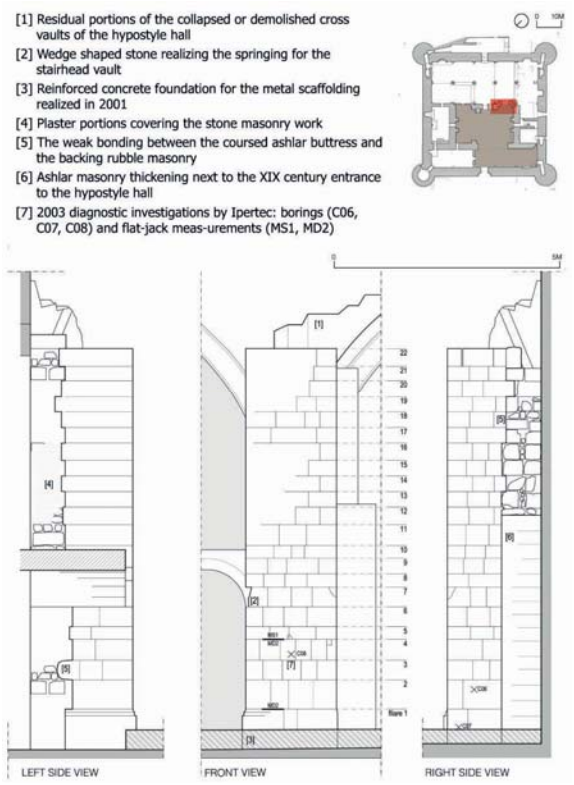

Figure 7 Survey of the right buttress. Both buttresses present a stonework arrangement with regular running bonds and headers forming a coursed ashlar with adequate grout core. They are juxtaposed with rougher masonry work in which the trilobate columns of the hall are partially embedded.

Figure 8 A lateral view of the stonework arrangement of the right buttress. From the top of the buttresses, the surviving *tas-de-charge* portions of the vaults, which collapsed or were demolished in the 18th century, can be seen.

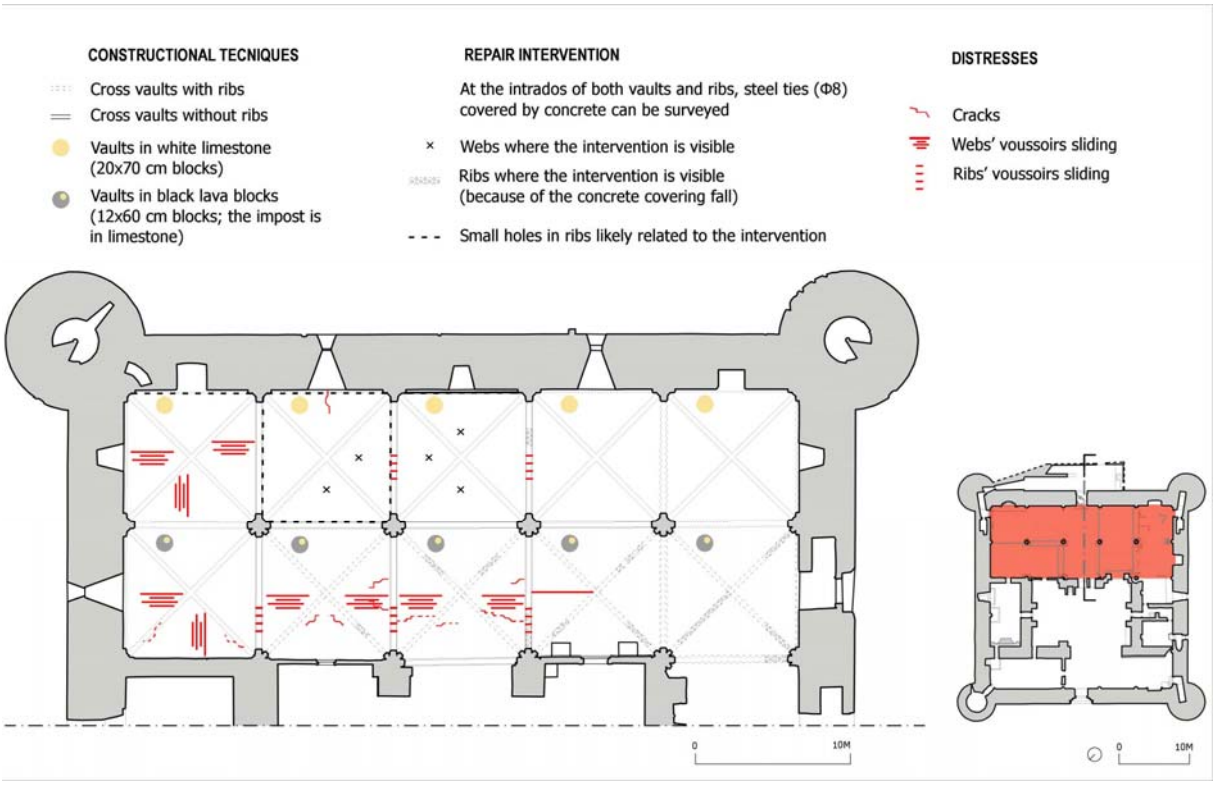

Figure 9 The crack pattern surveyed on the vaults' intrados is compatible with an outward movement of the courtyard façade due to the unbalanced thrust of the surviving vaults.

Figure 10 The classical sliding mechanism (as a consequence of the springing displacement) surveyed on the *voussoirs* of the pointed arches rising from the trilobate columns.

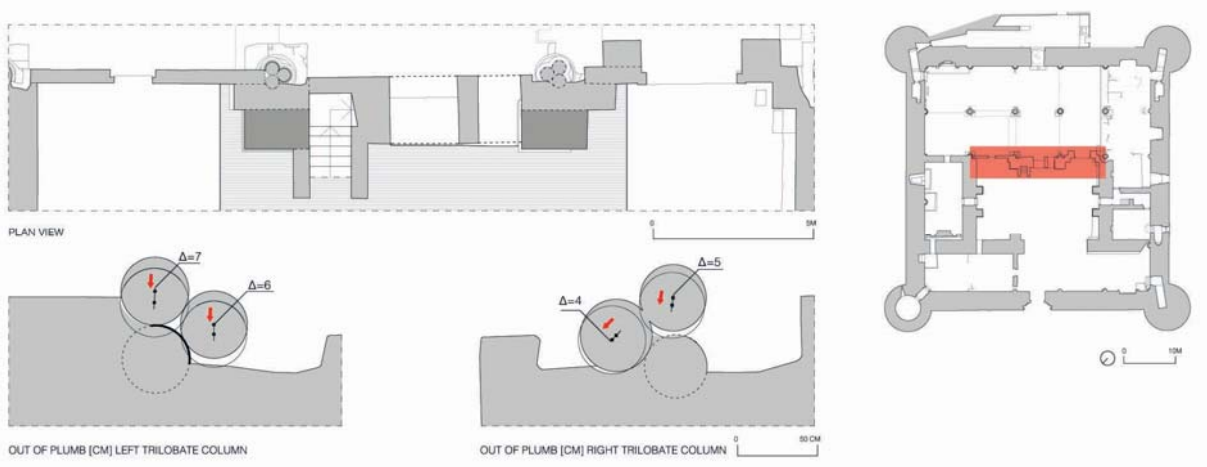

Figure 11 The out-of-plumb registered for both trilobate columns.

Figure 12 Cracks in the marble shafts of the trilobate columns deriving from the stress concentration due to eccentric axial loads.

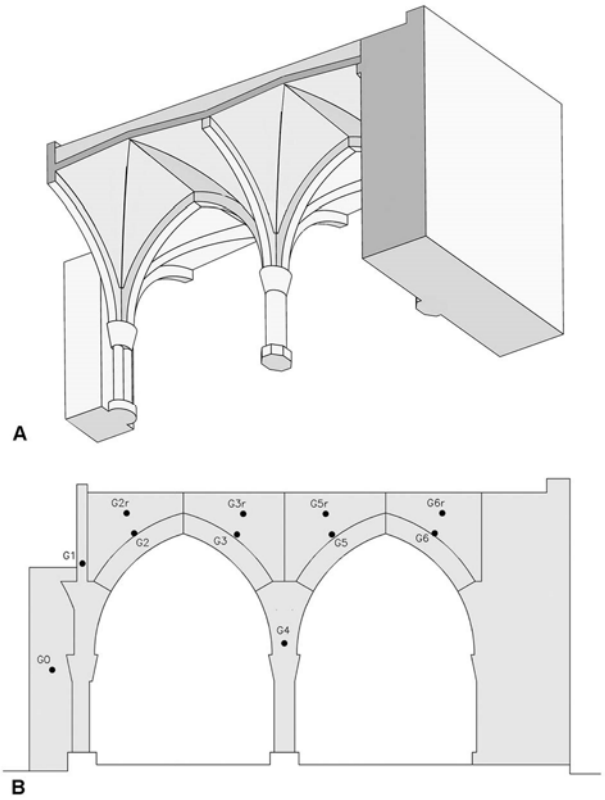

Figure 13 Structural section comprising vaults, trilobate columns and buttresses (A), and corresponding 2-D model with rigid body discretization and mass centres' position (B).

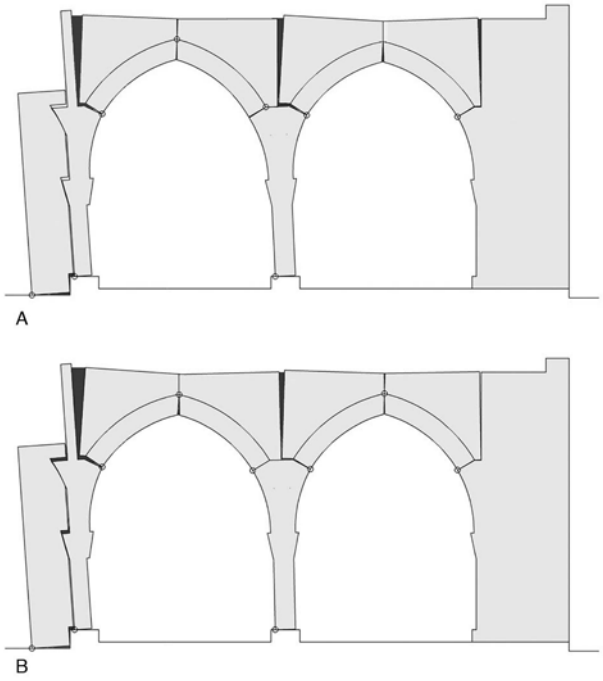

Figure 14 Critical kinematic mechanism detected in the analysis (A). The mechanism involves an intrados crack opening at the haunch of the left vault – unlike the classical flexural mechanism (B), which is nonetheless kinematically consistent – because it entails a larger outward rotation for the inner column and, consequently, a lower ultimate load factor.

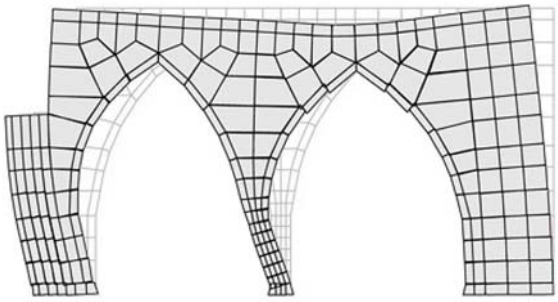

Figure 15 Collapse deformed shape obtained by FE analyses (Casolo and Sanjust 2009)

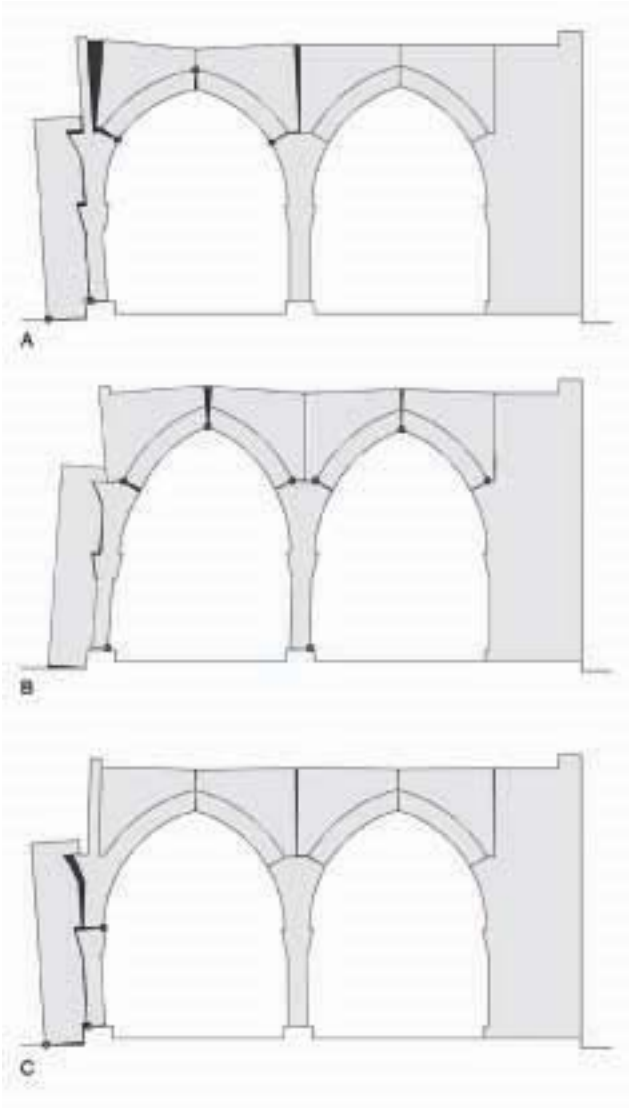

Figure 16 Different kinematic mechanisms checked in the analyses with hinges located so as to produce different crack openings.

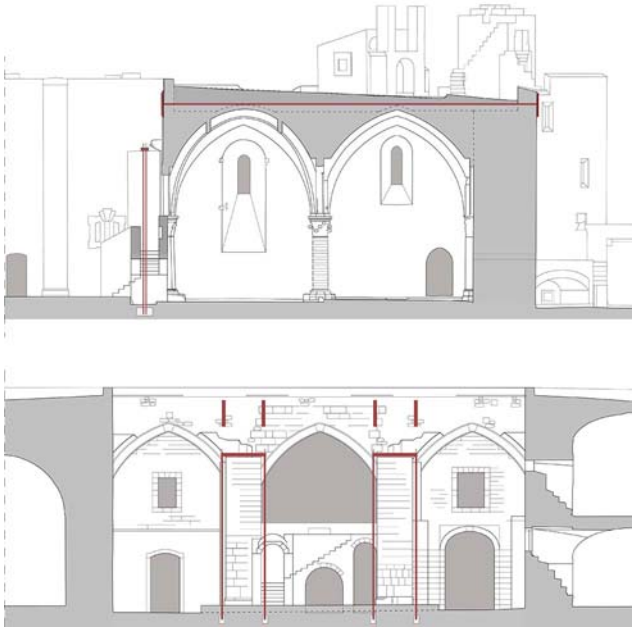

Figure 17 Elevation and transverse section of the proposed design solution with the vertical steel tendons on the sides of each buttress and the upper tie-rods anchoring the courtyard façade.

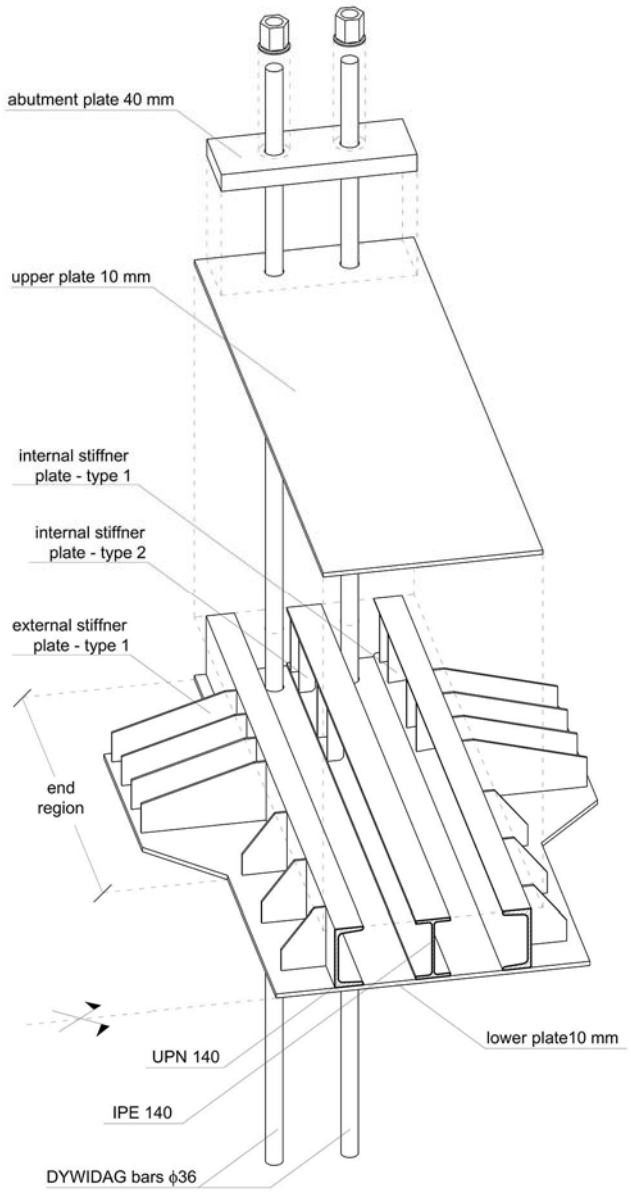

Figure 18 Exploded axonometric view of the upper anchorage system on the top of buttress

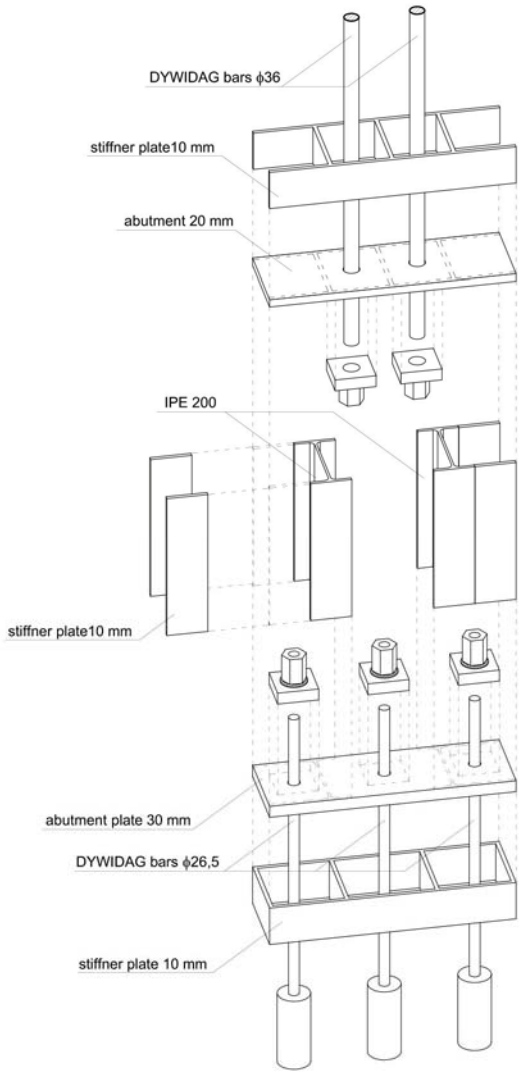

Figure 19 Steel joint hinge connection between tendons and piles.

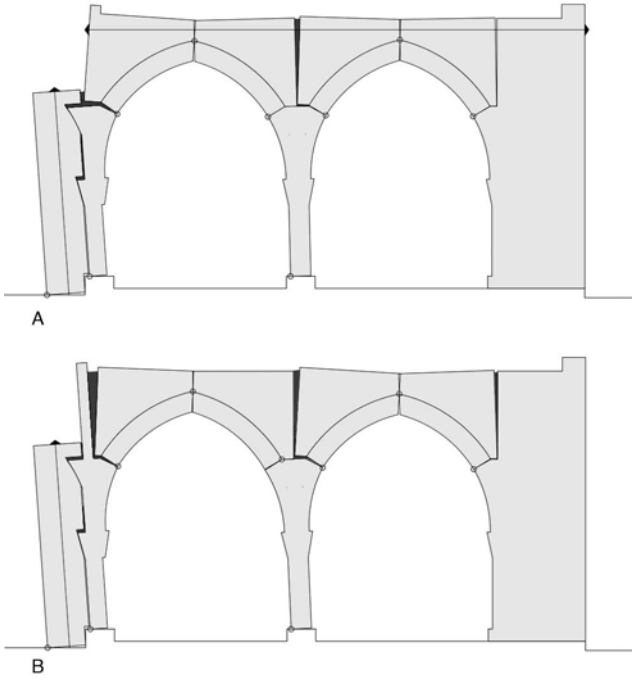

Figure 20 Kinematic analysis of the design solution: with both vertical tendons and horizontal tie-rods (A) and with vertical tendons only (B).

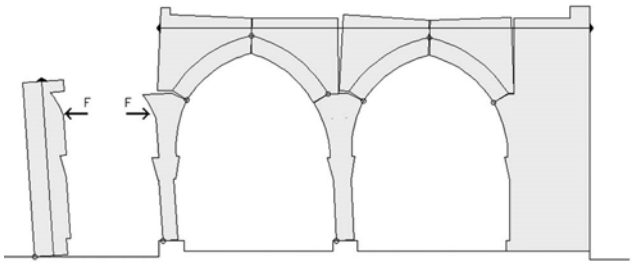

Figure 21 Simplified model (based on the equilibrium of sub-structures) singled out to evaluate horizontal force F which vaulted structures receive from (and transmit to) buttresses.

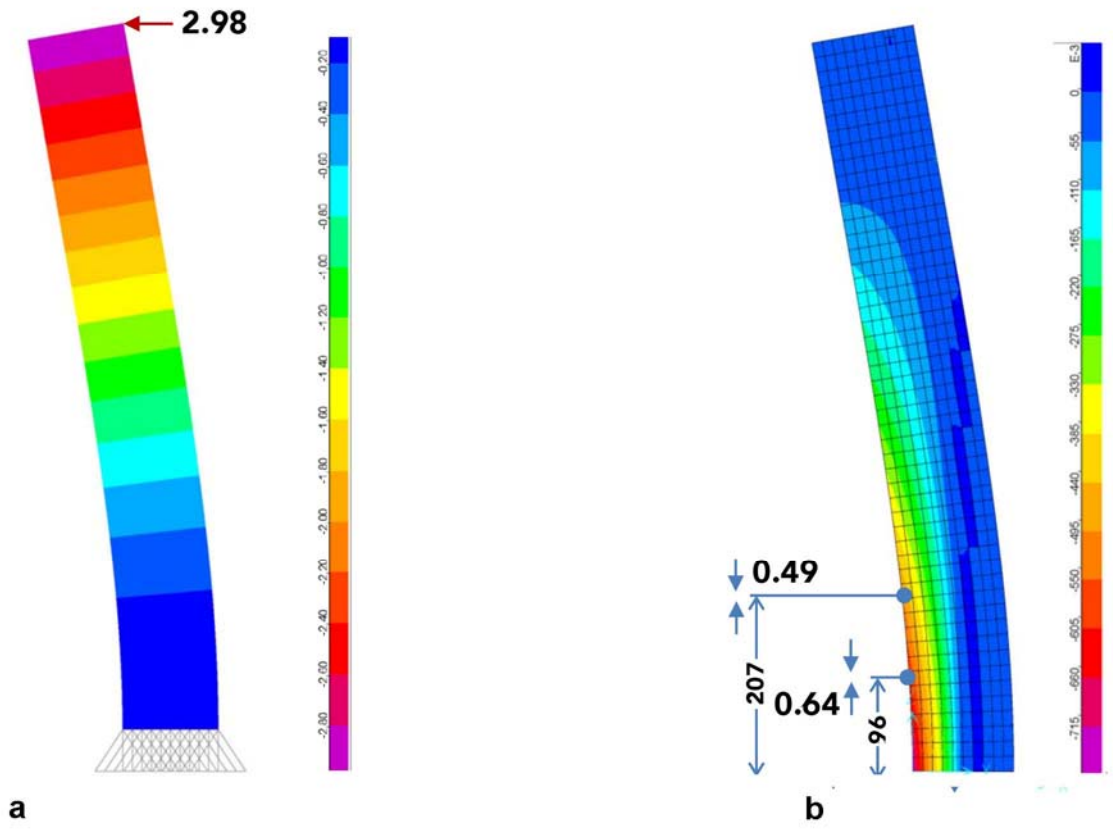

Figure 22 2-D non-linear analysis of the buttresses in the present configuration: displacement [mm] (a) and vertical stress [MPa] (b).

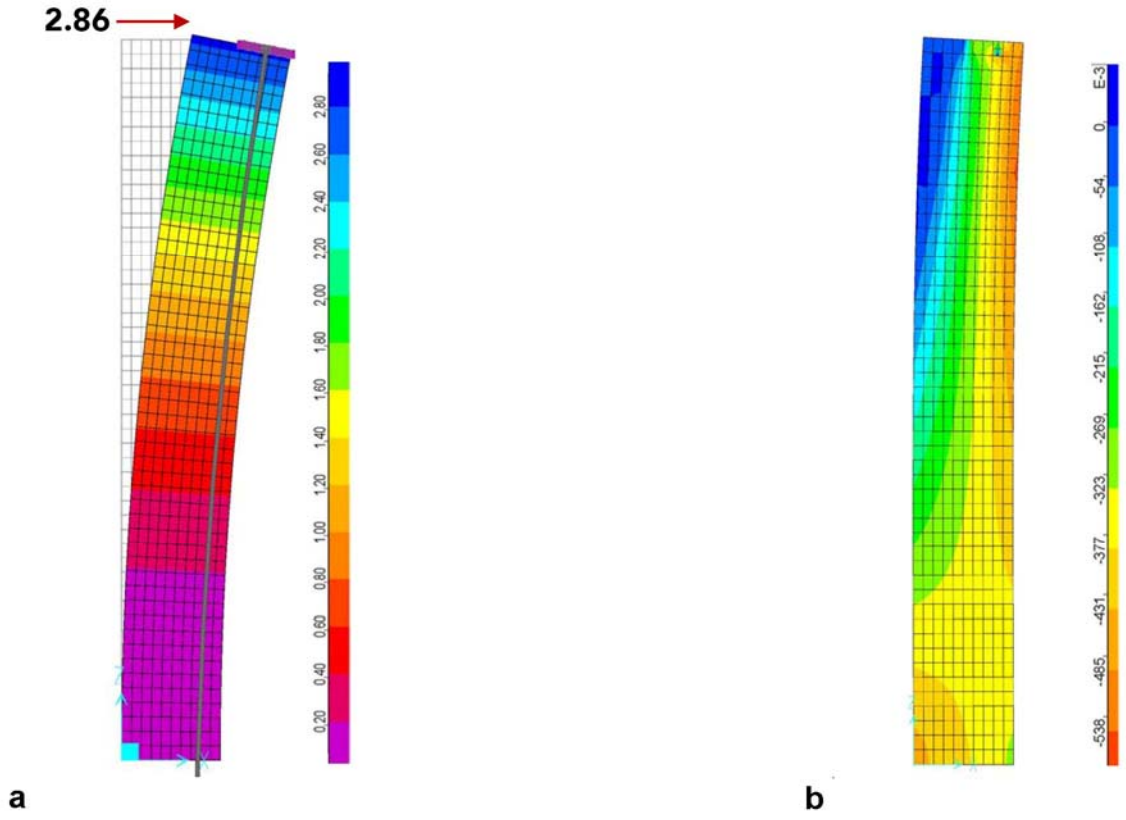

Figure 23 2-D non-linear analysis of the buttresses in the design configuration: displacement [mm] (a) and vertical stress [MPa] (b) for static loads.

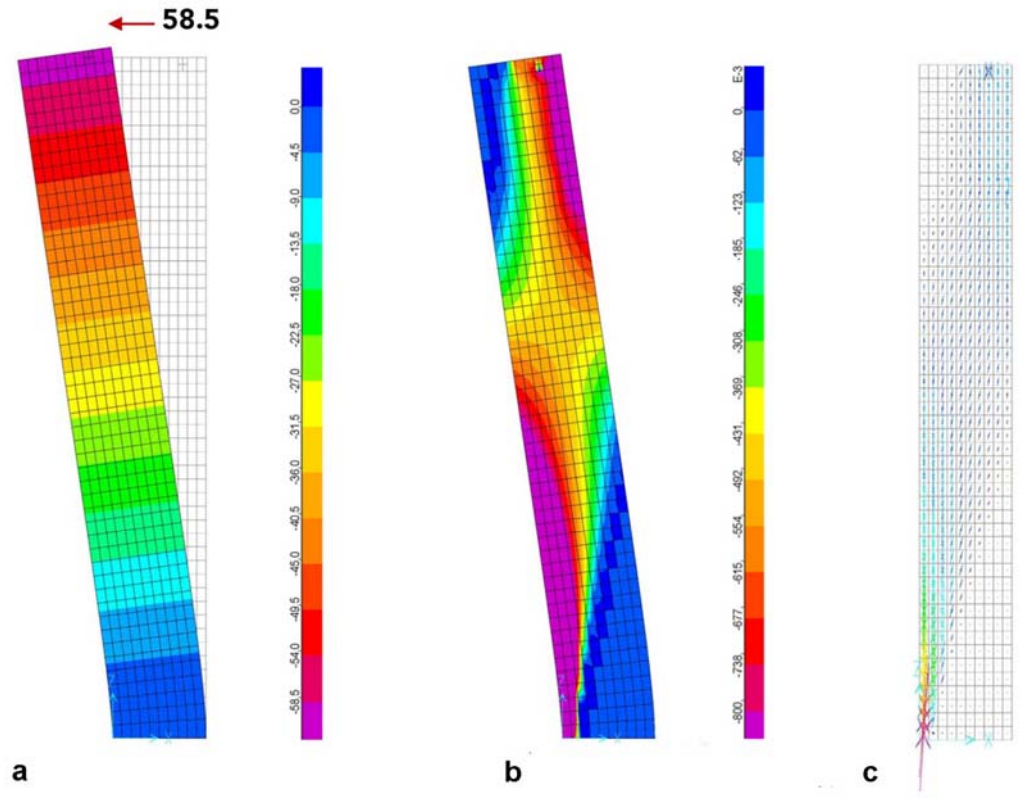

Figure 24 2-D non-linear analysis of the buttresses in the design configuration: displacement [mm] (a) and vertical stress [MPa] (b) under seismic action.

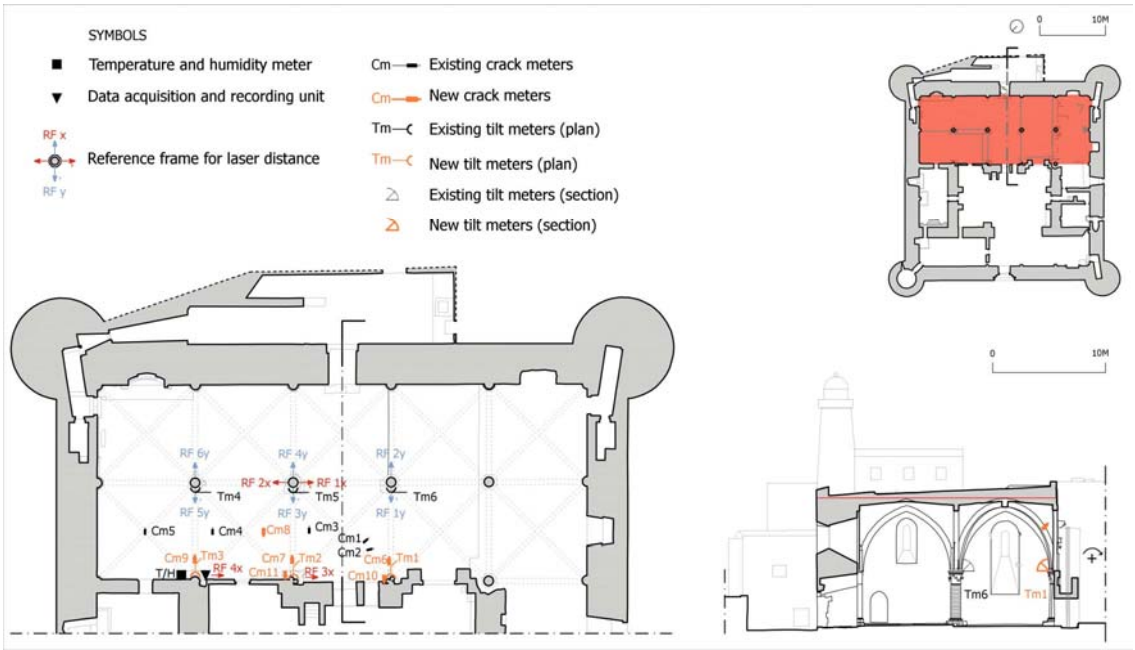

Figure 25 General layout of the monitoring devices.

Figure 26 Picture of the anchor plates to sustain the façade.

Figure 27 Picture of the stiffened top plate over the buttress, levelled by mortar ad a copper coating

Figure 28 The inclined plane fixed to the existing scaffolding employed to pull up the stiffened plate.

Figure 29 Side view of the right buttress with the tendons and the anchor bars aligned and bounded by static couplers.

Figure 30 The façade during scaffolding dismantling; only a portion is still present on the back of a buttress.

Figure 31 The removal of the scaffolding is complete and its concrete foundation almost demolished.

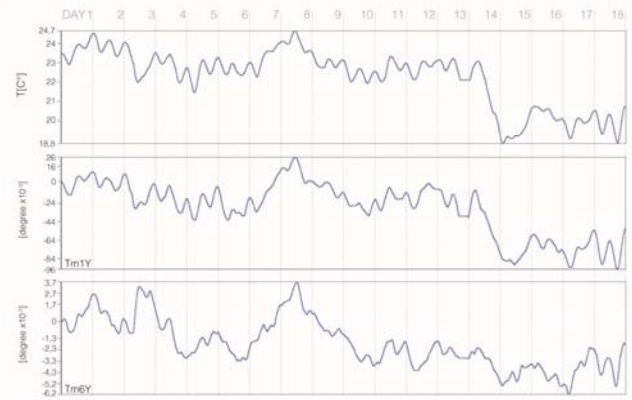

Figure 32 Data acquisition of temperature-gauge and tilt meters Tm1, Tm6 along y-direction for a time window covering major strengthening operations on the buttresses.